Macromolecular Research
https://doi.org/10.1007/s13233-023-00129-6

Online ISSN 2092-7673
Print ISSN 1598-5032

ARTICLE

New quinone-based electrode additives electrochemically polymerized on activated carbon electrodes for improved pseudocapacitance

Kyuchul Lee[1] · Jihyun Hwang[2] · Jeong Ho Park[2] · Jongwook Park[3] · Kangwon Lee[1,4] · Jang Myoun Ko[2]

Received: 12 August 2022 / Revised: 21 September 2022 / Accepted: 13 October 2022

Abstract

Three quinone-based derivatives (HBU680, HBU888, and HBU889) are synthesized and separately mixed with activated carbon (AC) and electropolymerized to form a homogeneous composite electrode. The electrochemical properties of the composite electrodes are studied. The electrochemical properties are mainly characterized by PhQ-PhQH2 and Q-QH2 redox transitions. The composite electrodes show specific capacitance of 176 F/g, 262 F/g, and 145 F/g for HBU680, HBU888, and HBU889, respectively. The HBU888 shows the highest specific capacitance due to the fast PhQ-PhQH2 redox transition at a scan rate of 100 mV/s. The composite electrodes also show a 100% capacity retention over 10,000 cycles. These results show that the new quinone-based derivates can enhance pseudocapacitive behavior and warrant their use as electrode additives for supercapacitors.

Graphical abstract

The new quinone-based electrode additives were synthesized and used as additives for supercapacitor electrodes. The electrochemical properties are mainly characterized by PhQ-PhQH2 and Q-QH2 redox transitions. The composite electrodes show specific capacitance of 176 F/g, 262 F/g, and 145 F/g for HBU680, HBU888, and HBU889 respectively. The HBU888 shows the highest specific capacitance due to the fast PhQ-PhQH2 redox. The composite electrodes also show a 100% capacity retention over 5000 cycles.

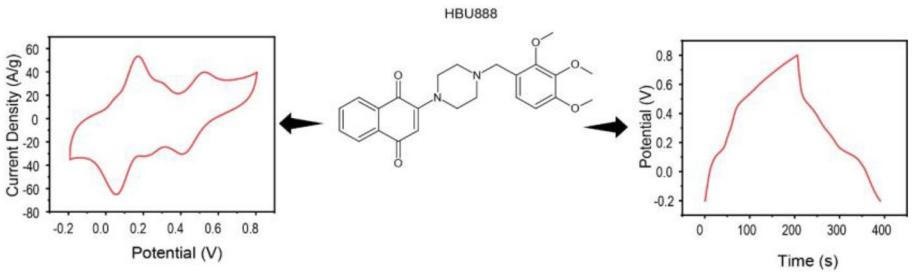

Keywords Quinone based · Activated carbon · Pseudocapacitance · Redox reaction

1 Introduction

Pseudo-supercapacitors also known as faradaic supercapacitors are a type of supercapacitors where the electrode materials, besides the electric double layer process, also undergo redox reactions making them behave more like batteries than supercapacitors [1, 2]. According to Conway et al., pseudocapacitance is defined as the electric power

✉ Jongwook Park
jongpark@khu.ac.kr

✉ Kangwon Lee
kangwonlee@snu.ac.kr

✉ Jang Myoun Ko
jmko@hanbat.ac.kr

Extended author information available on the last page of the article

Published online: 02 March 2023

that is stored in a pseudocapacitor through fast faradaic charge transfer [3]. This stored electric power is realized through a rapid sequence of redox reactions, electro-sorption, or intercalation processes on the electrodes [4]. The presence of pseudocapacitance can greatly increase the energy density of supercapacitors, while cycling stability is still favored [1, 5]. The choice of electrolyte plays a very important role in the overall specific capacitance obtained from electrode materials. Electrolytes are divided into two groups which are, aprotic and protic electrolytes. They each have their advantages and disadvantages. Protic electrolytes, which are usually polymers, salts, acids, and bases dissolved in water, are generally environmentally friendly, safer, and have higher ionic conductivity. On the other hand, aprotic electrolytes, which are usually salts or polymers dissolved in carbonate solvents or ionic liquids, are usually environmentally unfriendly and toxic, however, they have a wider working voltage window [3, 6].

Some of the electrode materials used in pseudocapacitors include metal oxides such as ruthenium oxide (RuO_2), manganese dioxide (MnO), etc. [4, 7] However, such materials are expensive and undergo slow redox reactions thus the use of quinone-based derivatives as additives in activated carbon (AC) electrodes [8, 9]. Quinone-based derivatives will introduce sites for fast redox reactions as potential is applied to the system [8–11]. In the previous work by S. Sathymoorthi et al., it was noticeable that quinone-containing organic species enhance the electrochemical properties through their redox-active behaviors via a quinone-hydroquinone transition [8, 12]. An activated carbon supercapacitor with 2,5-bis((2-(1H-indol-3-yl)ethyl)amino) cyclohexa-2,5-diene-1,4-dione (HBU), had a specific capacitance of 130 F/g at 100 mV/s [9]. However, quinone-based derivatives can dissolve in non-aqueous electrolytes leading to rapid capacity degradation, self-discharge, and poor coulombic efficiency [13, 14]. To buttress this, the quinone-based derivatives can be immobilized onto the surface of the electrode by grafting onto a carbon base or electropolymerization of the grafted quinone derivative monomer [15]. Once polymerized, the derivative becomes immune to dissolution. In this polymerized state, the quinone-based derivatives maintain their redox properties [16] thus they can still induce pseudocapacitance when electropolymerized on activated carbon.

In this study, three new quinone-based derivatives are synthesized and coupled with activated carbon as pseudocapacitor electrodes. Upon charging, the quinone-based derivatives are electropolymerized forming a passivation layer with redox properties that enhances the pseudocapacitive behavior of the electrode. Electrochemical tests were performed to determine their effects on capacitance and cycle performance.

2 Experimental

2.1 Synthesis of HBU889

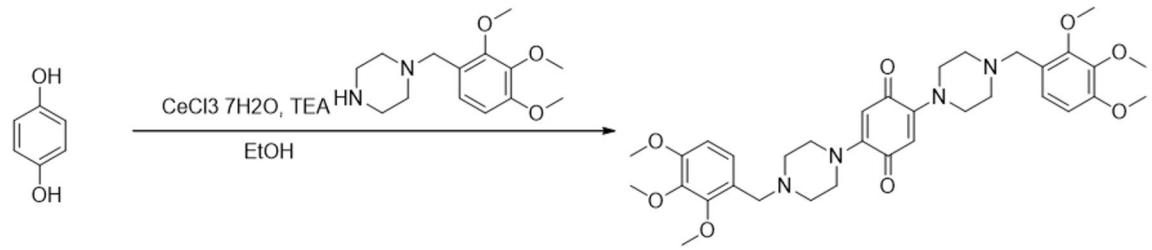

Hydroquinone (200 mg, 1.82 mmol) was dissolved in EtOH, and $CeCl_3$ $7H_2O$ (67 mg, 0.18 mmol) was added. Subsequently, after adding 2,3,4-trimethoxy benzylpiperazine (1.24 g, 3.64 mmol) under an ice bath, TEA (1.27 ml, 9.1 mmol) was added drop wise. After overnight and concentration under reduced pressure, the reaction was terminated using H_2O under an ice bath. Subsequently, the brown solid was obtained through filtering (750 mg, 64.72% yield). The synthesized HBU additives were analyzed using ^1H and ^{13}C nuclear magnetic resonance (^1H NMR) spectroscopy (Varian Gemini 200 NMR) and mass spec, which was identified as follows: ^1H NMR(400 MHz, DMSO) 3.03 (t, J = 7.6 Hz, 2H), 3.48 (q, J = 6.8 Hz ^1H NMR (400 MHz, $CDCl_3$) δ 2.56 (s, 8H), 3.49 (s, 4H), 3.55 (s, 8H), 3.85 (s, 6H), 3.87 (d, J = 3.6, 12H), 5.50 (s, 2H), 6.63 (d, J = 8.4, 2H), 6.96 (d, J = 8.4, 2H); ^{13}C NMR ($CDCl_3$, 100 MHz) δ 48.92(2C), 52.54 (2C), 56.00 (2C), 56.41 (1C), 60.81 (2C), 61.22 (2C), 76.74 (4C), 77.06 (4C), 77.37 (4C), 106.55 (1C), 106.99 (2C), 123.41 (1C), 125.16 (2C), 142.34 (1C), 152.34 (2C), 153.09 (1C), 182.68 (1C); ESI–MS: m/z [M] + 637.3 (calcd. 636.74).

2.2 Synthesis of HBU888

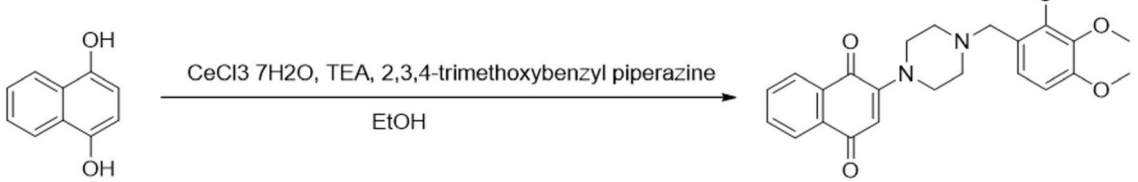

1,4,-Dihydroxy naphthalene (200 mg, 1.20 mmol) was dissolved in ethanol, and $CeCl_3$ $7H_2O$ (45 mg, 0.12 mmol) was added. Subsequently, after adding 2,3,4-trimethoxybenzyl piperazine (410 mg, 1.20 mmol) under an ice bath, TEA (500 ml, 3.6 mmol) was added dropwise. After overnight and concentration under reduced pressure, the reaction was terminated using H_2O under an ice bath. After filtering the solid, the obtained solid was dissolved in acetone, concentrated under reduced pressure, and recrystallized from ether. The crude liquid was collected and concentrated under reduced pressure by column chromatography (DCM → DCM: MeOH = 19:1) to obtain (dark red liquid, 76 mg, 14.99% yield). TLC 〔EA:HEX = 1:1 Rf = 0.4; ^1H NMR (400 MHz, $CDCl_3$) δ 2.63(t, J = 4.8 Hz, 4H), 3.51 ~ 3.53 (m, 6H), 3.86 (s, 3H), 3.88 (s, 3H), 3.90 (s, 3H), 6.00 (s, 1H), 6.65(d, J = 8.8 Hz, 1H), 6.99(d, J = 8.4 Hz, 1H), 7.62 (td, J = 1.2 Hz, J = 7.6 Hz, 1H), 7.63 (td, J = 1.2 Hz, J = 7.6 Hz, 1H), 7.99 (dd, J = 0.8 Hz, J = 7.6 Hz, 1H), 8.03 (dd, J = 0.8 Hz, J = 7.6 Hz, 1H); ^{13}C NMR ($CDCl_3$, 100 MHz) δ 49.03 (2C), 52.42 (2C), 55.99 (1C), 56.43 (1C), 60.80 (1C), 61.22 (1C), 107.00 (1C), 111.47 (1C), 123.30 (1C), 125.17 (1C), 125.52 (1C), 126.65 (1C), 132.40 (1C), 132.84 (2C), 133.83 (1C), 142.34 (1C), 152.67 (1C), 153.12 (1C), 153.80 (1C), 183.11 (1C), 183.64 (1C); ESI–MS: m/z [M] + 423.2 (calcd. 422.18).

2.3 Synthesis of HBU680

2.3.1 1-(Azidomethyl)-3-methoxybenzene

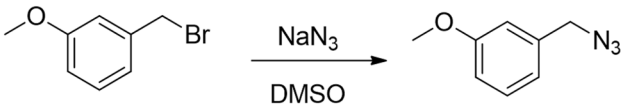

3-Methoxybenzyl bromide (0.19 mL, 1.27 mmol) was dissolved in 10 mL of DMSO, and NaN_3 was added in small portions. Subsequently, the mixture was stirred at room temperature for 24 h. After terminating the reaction with H_2O, the organic layer was extracted with ether. The extracted organic layer was filtered under reduced pressure after water removal with anhydrous $MgSO_4$ to obtain a solution. This was concentrated under reduced pressure to obtain a colorless liquid. (150 mg, 92%). ^1H NMR ($CDCl_3$, 400 MHz) δ 3.80 (s, 3H), 4.29 (s, 2H), 6.85 ~ 6.89 (m, 3H), 7.28 (t, J = 8.0 Hz, 1H).

2.3.2 6-(((1-(3-Methoxybenzyl)-1H-1,2,3-triazole-4-yl) methyl)amino)-6H-dibenzo[c,e][1,2] oxaphosphinine 6-oxide

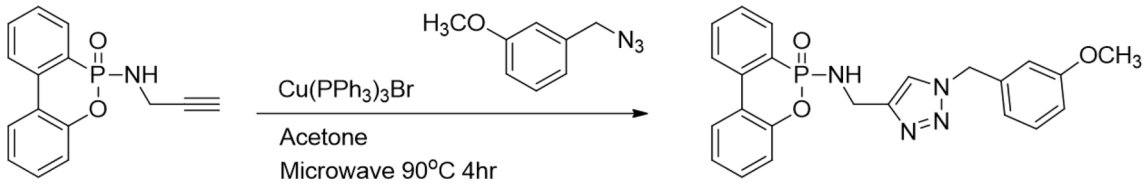

6-(Ethynylamino)-6H-dibenzo[c,e][1,2]oxaphosphinine 6-oxide (0.20 g, 0.74 mmol) was dissolved in acetone solvent, then $Cu(PPh_3)_3Br$ (0.07 g, 0.074 mmol) and 1-(Azidomethyl)-3-methoxybenzene (0.13 g, 0.82 mmol) were added into the solution. Subsequently, the mixture was reacted in a microwave at 90 °C for 4 h. After separation by column chromatography (DCM: MeOH 40:1), a brown solid (260 mg, 81% yield) was obtained. ^{1}H NMR (DMSO-d_6, 400 MHz) δ 3.75 (s, 3H), 4.09 (d, J = 7.2 Hz, 1H), 4.13 (d, J = 7.2 Hz, 1H) 5.55 (s, 2H), 6.24 (m, 1H), 6.89 (d, J = 7.6 Hz, 1H), 6.93 (t, J = 2.4 Hz, 2H), 7.16 (d, J = 8.0 Hz, 1H), 7.20 (d, J = 6.8 Hz, 1H), 7.33 (d, J = 7.6 Hz, 1H) 7.42 (t, J = 8.0 Hz, 1H), 7.51 (td J = 2.8, 7.6 Hz, 1H), 7.74 (d, J = 7.6 Hz, 1H), 7.77 (d, J = 7.6 Hz, 1H) 7.98 (s, 1H), 8.16 ~ 8.21 (m, 2H); ^{13}C NMR (DMSO-d_6, 100 MHz) δ 36.30, 53.16, 55.61, 113.86, 114.37, 120.56 (d, J = 6.0 Hz), 120.58, 122.46 (d, J = 12.0 Hz), 123.57, 124.53 (d, J = 10.0 Hz), 124.75, 125.90, 125.92 (d, J = 161.0 Hz), 128.75, 130.04 (d, J = 10.0 Hz), 130.38, 130.82, 133.21, 133.23, 136.45 (d, J = 7.0 Hz), 138.04, 149.89 (d, J = 7.0 Hz), 159.94 Melting point (℃) 50℃; ESI–MS: m/z $[M+H]^+$ 433.2(calcd. 432.14).

2.4 Composite electrode preparation and measurement

HBU680, HBU888, and HBU889 were used as redox additives separately for supercapacitor electrodes. The viscous electrode slurry was prepared by mixing AC (MSC-30, Kansai Cokes, 70 wt.%), synthesized quinine-based additives (25 wt.%), and polymeric binder (polyvinylidene fluoride (Aldrich, 5 wt.%) and N-methyl-2-pyrrolidinone as the dispersion solvent. The viscous slurries for the AC and each composite sample were coated individually on platinum current collectors. The dimensions of platinum current collectors measured 1.0 cm × 1.0 cm. They were dried at 100 °C in an oven for 4 h to evaporate the solvent component [17].

Table 1 BET results for surface area, pore volume, and pore size of the samples

Sample	Surface area ($m^2\ g^{-1}$)	Pore volume ($cm^2\ g^{-1}$)	Pore size (nm)
AC	212	0.09	2.11
HBU889	255	0.13	1.45
HBU888	425	0.16	1.69
HBU680	373	0.14	1.59

2.5 Composite powder and electrode characterization

Scanning electron microscopy (SEM) images and Brunauer–Emmett–Teller (BET) analysis were done using a Hitachi S-4800 field emission scanning electron microscopy (FESEM) and a Tristar II 3020 Micromeritics instrument, respectively. For electrochemical measurements, an Autolab PGstat 100, Eco Chemie was used. A three-electrode cell was applied with Ag/AgCl saturated with KCl as a reference electrode, platinum as a counter electrode, and the as-prepared electrodes as a working electrode. 1 M H_2SO_4 was used as an electrolyte. Cyclic voltammetry (CV) was conducted at different scan rates ranging from 100 to 1000 mV/s. Galvanostatic charge–discharge (CD) was carried out at different current densities of 5, 7, and 10 mA/cm^2. All tests were done in the potential range of – 0.2 to 0.8 V. The specific capacitance (Cs) of the electrodes was calculated as a function of scan rate using equation.

$$CS = \frac{[Q1 + Q2]}{2m\Delta V},$$

where Cs is the specific capacitance, Q1 anodic charge, Q2 cathodic charge, ΔV is the potential window used, and m mass of active material.

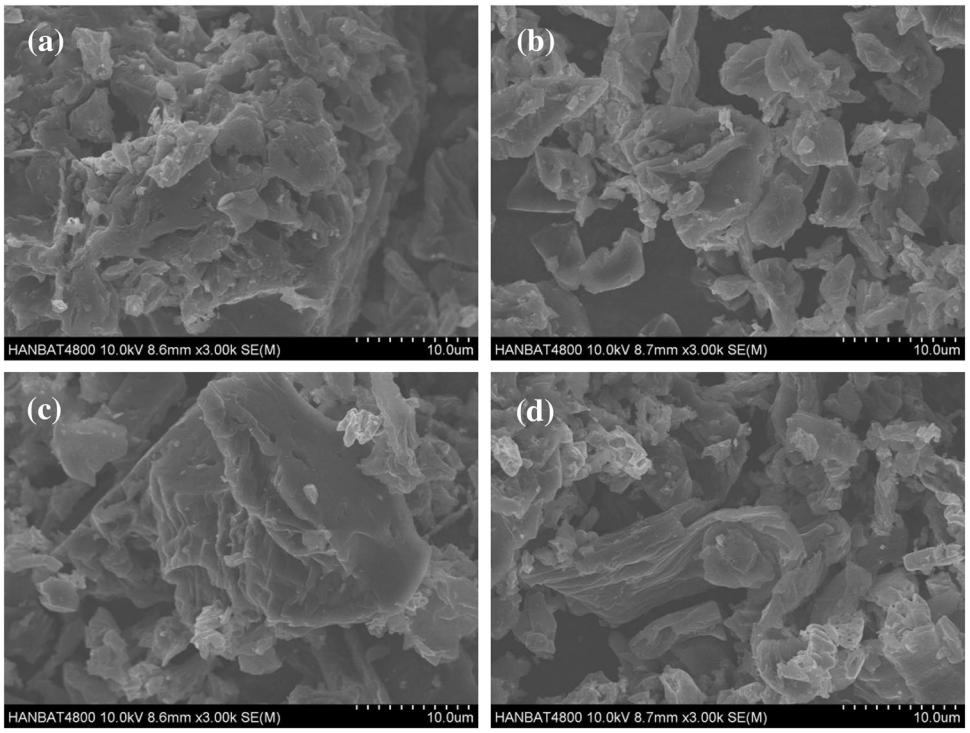

Fig. 1 SEM images for **a** AC, **b** HBU889, **c** HBU888, and **d** HBU680

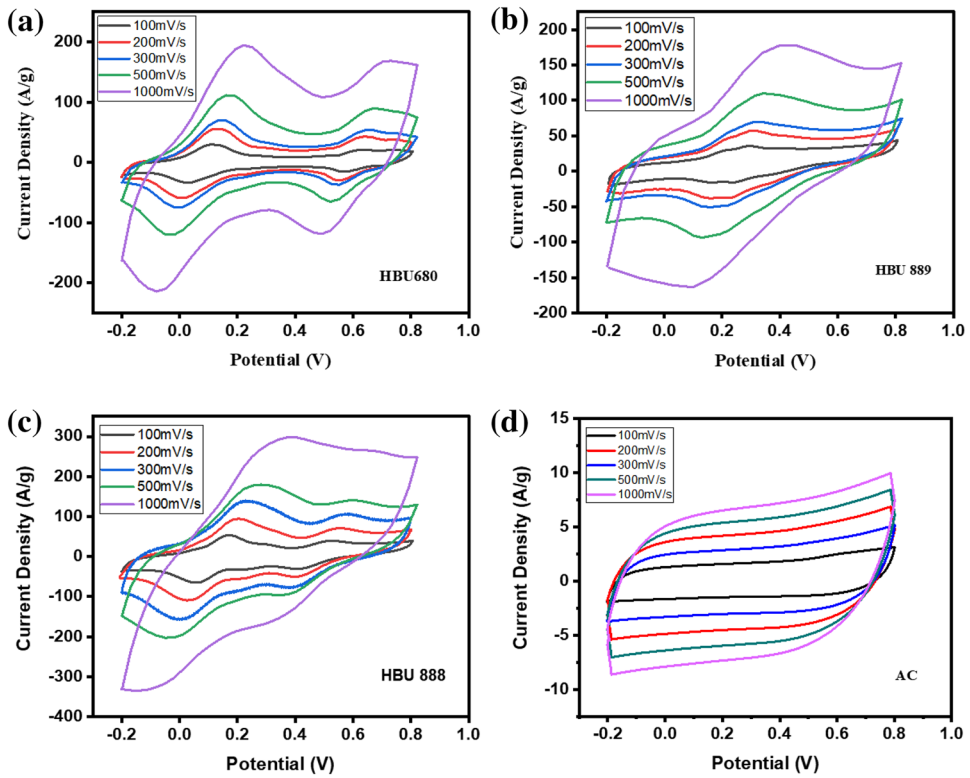

Fig. 2 CVs for **a** HBU680, **b** HBU889, **c** HBU888, and **d** AC electrodes at various scan rates

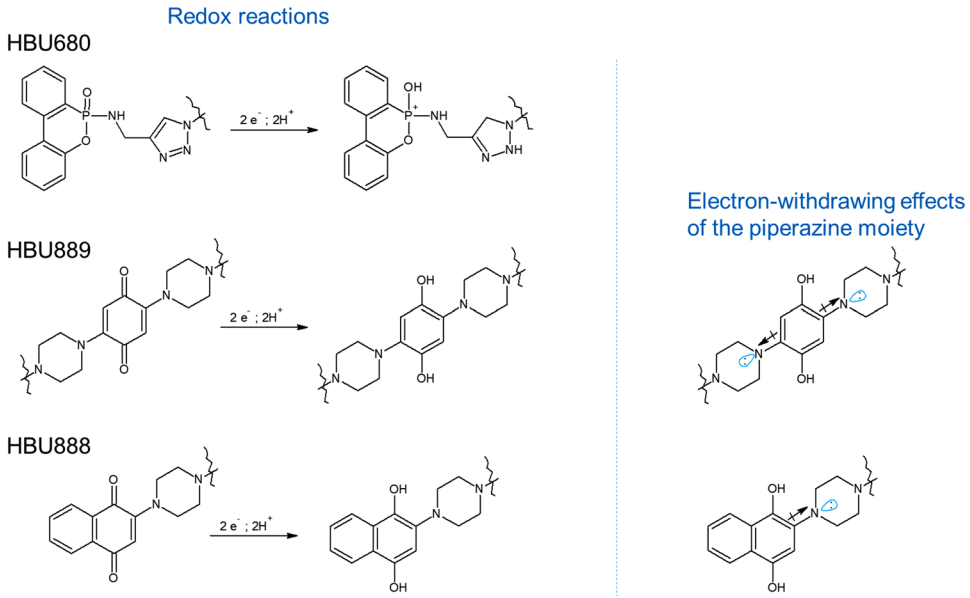

Fig. 3 Redox mechanisms of the HBU additives

3 Results and discussion

The N_2 adsorption–desorption isotherm was used to determine the pore size and specific surface area of the as-prepared AC (Supplementary Figure S1). The results from the graphs show an inverse relationship between the relative pressure and the volume. At low relative pressure (P/P_0), there is an increase in adsorption volume. Isotherms reach a plateau in the middle and have high relative pressure. This behavior suggests the presence of micropores. Upon electropolymerization, a thin, porous, and passivation film is formed and anchored [17–19] on the surface of the AC particles. Once the layer is formed; it blocks further polymerization of other monomers that are covered by it thus self-limiting [18, 20]. The porosity of the electrodes then depends on the degree of polymerization, and the structure and permeability of the polymer layer covering the AC particles [20]. The isotherms were further analyzed for pore size distribution [9]. Table 1 presents the summary of the surface area, pore volume, and pore size of the different samples. The surface area follows the trend HBU888 > HBU680 > HBU889 > AC. This shows that the addition of HBU samples enhances surface area perhaps due to the addition of more organic material on the surface of the electrode. The enhanced specific surface area of HBU888 enables it to have (i) improved ion migration, and (ii) more active sites for electric double layer and redox processes hence enhanced electrochemical performance [9, 21, 22].

SEM images of the various samples are presented in Fig. 1. The SEM images of all the samples display mesopores with non-uniform intercellular spaces. This shows that the addition of the HBU additives and the electropolymerization did not affect the morphological structure of the activated carbon [11]. Furthermore, the mixing of the HBU samples with the AC produced a homogenous mixture resulting in a well-mixed electrode. This helps to facilitate even coverage of the AC particles by the thin polymer film upon electropolymerization. This leads to a smooth synergy of electric double layer and faradaic processes on the electrode surface thereby enhancing electrochemical performance [9, 11].

Figure 2 displays CV analysis for AC and the three additives HBU680, HBU888, and HBU889 carried out in 1 M H_2SO_4 at a scan rate range from 100 mV/s to 1000 mV/s. The CVs for the HBU samples show both electric double-layer behavior and double redox peaks due to the redox reaction of the quinone-based additives [2]. The HBU680 undergoes a redox reaction at the O atom double-bonded to the P on the DOPO PP and the middle N atom in the triazole structure. The more electronegative N pulls electrons from the double bond towards itself resulting in a partial negative charge where the H^+ ion can reversibly bond to make a secondary amine group (NH group) [11, 22, 23]. The oxide ion bonded to P due to resonance will become a hydroxyl anion. This enhances the specific capacitance compared to pure AC. However, it has the lowest specific capacitance compared to the other HBU additives due to the slowness of the redox reactions on the redox-active sites (the P=O and =N–N=N–) despite the differences in capacitance.

The basicity of phosphoxide and the aromatic N is lower compared to that of the phenoxide anion formed by the quinone moiety. The HBU889 undergoes the quinone–hydroquinone (Q-QH_2) transition with hydroquinone in an acidic medium. There are no aromatic N groups but rather two

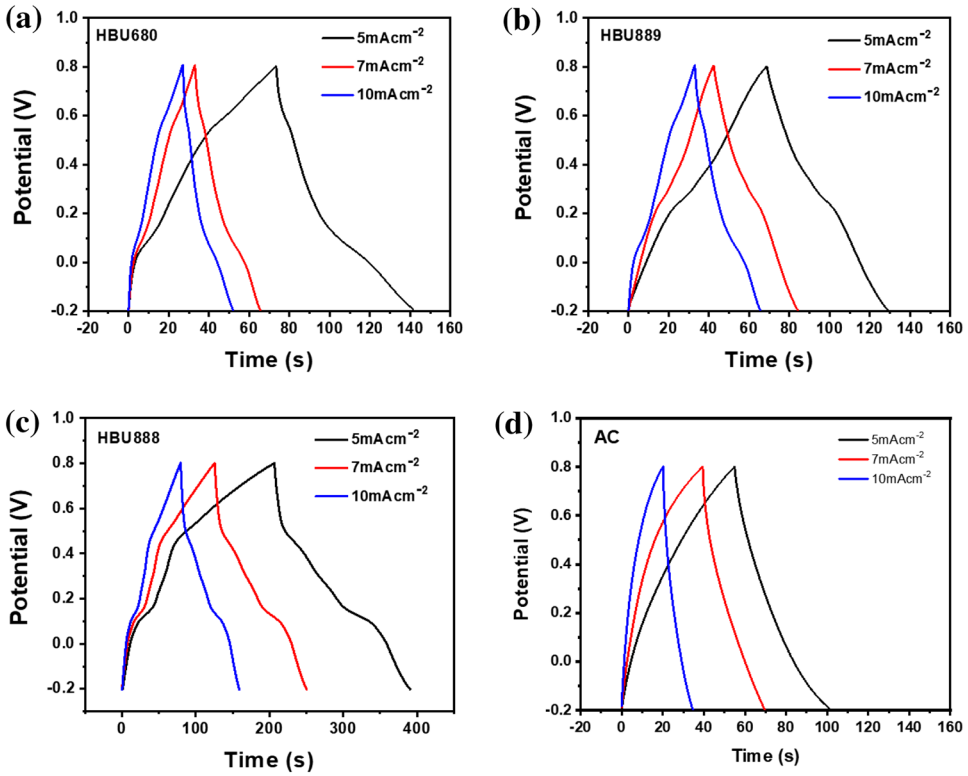

Fig. 4 Charge/discharge profiles for **a** HBU680, **b** HBU889, **c** HBU888, and **d** AC electrodes at various current densities

Table 2 Summary of specific capacitance

Sample	Specific capacitance @100mVs^{-1}
HBU888	262
HBU889	145
HBU680	176
AC	83

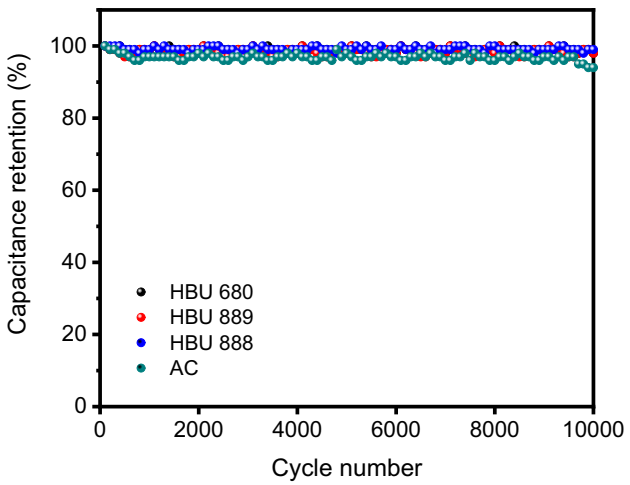

Fig. 5 Long-term cycle capacity retention of the different electrodes

2,3,4-trimethoxybenzylpiperazine groups directly bonded to the quinone moiety. The piperazine nitrogen atoms do not enhance the π-system in the quinone benzene ring but electron-withdrawing since they are tertiary N atoms [24, 25]. This reduces and destabilizes the quinone -system thereby reducing its basicity and resulting in a reduced rate of the PhQ-PhQH$_2$ transition thus less redox active compared to that of HBU888 (Fig. 3). Furthermore, the presence of additional aromatic rings has a negative effect on the half-wave potentials in CV [5]. On the other hand, HBU888 displayed the highest specific capacitance. Like HBU889, it undergoes PhQ-PhQH$_2$ transition, however, the side groups on the quinone moiety are different. It has one 2,3,4-trimethoxybenzylpiperazine group thus less electron-withdrawing hence more basic than HBU889 [11]. Furthermore, another reason for the high capacitance displayed by the electrodes with HBU888 could be that the polymer formed upon electropolymerization was more permeable for electrolyte ions [15]. This enables more ions to be in contact with the electrode surface thus enhancing the capacitance. Pure AC has the lowest specific capacitance because it only has the electric double layer process [26]. However, the combination of AC and the HBU additives produces pseudocapacitive behavior. The HBU additives can homogenize with the AC particles due to (i) anchoring on the AC particles upon electropolymerization and (ii) the unpolymerized HBU monomers can form intermolecular forces of attraction with the surface of

the activated carbon that contains other functional groups such as amine, hydroxyl, carboxylic, carbonyl and aromatic groups. This helps to merge the electric double layer and faradaic process within the electrode resulting in improved electron delocalization and charge transfer kinetics [11, 27].

Figure 4 shows the charge–discharge profiles for the four samples. At a constant current density of 5 mA cm^{-1}, the HBU680, HBU889, HBU888, and AC had an average charge–discharge time of 141, 129, 391, and 101 s mg^{-1}, respectively. The HBU 888 had the longest cycle time implying a higher specific capacitance which is in agrees with the CV curves in Fig. 2. Furthermore, the HBU888 profile has more defined peak shoulders compared to HBU680 and HBU889 implying a more pronounced redox reaction [28]. The summary of the specific capacitances is shown in Table 2. Figure 5 shows the long cycle capacity retention. All the samples display capacity retention > 99% over 10 000 cycles. This shows that the new HBU additives are (i) chemically stable for long-term cycling and (ii) can be electrochemically polymerized with little effect on their electrochemical performance. Thus, they have no negative effect on the cycle performance of the AC.

These results suggest that the new HBU additives can enhance the specific capacitance of AC with HBU888 having the best performance. The ability of the HBU additives to (i) electrochemically polymerize on the surface of the AC particles thereby anchoring them, (ii) binds to the surface of the AC by forming electrostatic forces of attraction, enhances the cooperation of the electric double layer, and faradaic process and (ii) undergo fast redox reaction enables then to positively influence the electrochemical properties of the composite electrodes.

4 Conclusions

The new quinone-based electrode additives HBU680, HBU889, and HBU889 were synthesized and used as additives for supercapacitor electrodes. The HBU680 was characterized by redox reactions of the NH group in the triazole ring and the oxide ion which yielded a specific capacitance of 176 F/g at a scan rate of 100 mV/s. HBU888 undergoes the PhQ-$PhQH_2$ transition and had the highest capacitance of 262 F/g at a scan rate of 100 mV/s. HBU889 had the least super capacitance of 145 F/g at a scan rate of 100 mV/s. The redox reactions were the Q-QH_2 transitions for HBU889. The galvanostatic results obtained showed that the HBU888 was the ideal organic additive as it had the longest cycle time which was more than double that of HBU889 and HBU680 at a constant current density of 5 $mAcm^{-1}$. The electrochemical polymerization of these new quinone-based derivatives has little to no effect on the electrochemical performance of the electrode. This study shows that chemically synthesized organic additives have a positive effect on the specific capacitance in supercapacitors hence they are promising candidates for use as electrode additives.

Supplementary Information The online version contains supplementary material available at https://doi.org/10.1007/s13233-023-00129-6.

Acknowledgements This research was supported by Basic Science Research Program through the National Research Foundation of Korea (NRF) funded by the Ministry of Education (2017R1D1A1B04028757). This research was supported by the Basic Science Research Program through the National Research Foundation of Korea (NRF) funded by the Ministry of Education (2020R1A6A1A03048004). This research was supported by Basic Science Research Capacity Enhancement Project through the Korea Basic Science Institute (National Research Facilities and Equipment Center) grant funded by the Ministry of Education (No. 2019R1A6C1010052).

References

1. Y. Liu, S.P. Jiang, Z. Shao, Mater. Today Adv. **7**, 100072 (2020)
2. J.S. Ko, M.B. Sassin, D.R. Rolison, J.W. Long, Electrochim. Acta. **275**, 225–235 (2018)
3. J. Libich, J. Máca, J. Vondrák, O. Čech, M. Sedlaříková, J. Energy Storage. **17**, 224–227 (2018)
4. J. Wang, S. Dong, B. Ding, Y. Wang, X. Hao, H. Dou, Y. Xia, X. Zhang, Natl. Sci. Rev. **4**, 71–90 (2017)
5. Y. Jiang, J. Liu, Energy Environ. Mater. **2**, 30 (2019)
6. I. Phiri, C.Y. Bon, S. Kim, M. Mwemezi, L. Hamenu, A. Madzvamuse, S.H. Kim, J.M. Ko, Curr. Appl. Phys. **20**, 122–131 (2020)
7. S. Fleischmann, J.B. Mitchell, R. Wang, C. Zhan, D.E. Jiang, V. Presser, V. Augustyn, Chem. Rev. **120**, 6738–6782 (2020)
8. S. Suematsu, K. Naoi, J. Power Sources. **816**, 97–98 (2001)
9. M. Latifatu, J.H. Park, J.M. Ko, J. Park, J. Ind. Eng. Chem. **63**, 12–18 (2018)
10. H. Lee, M. Suzuki, J. Cui, S.A. Kozmin, J. Org. Chem. **75**, 1756–1759 (2010)
11. H.S. Lee, M. Latifatu, B.C. Kim, J.H. Park, Y.G. Lee, K.M. Kim, J. Park, Y.G. Baek, J.M. Ko, Synth. Met. **217**, 29–36 (2016)
12. S. Sathyamoorthi, V. Suryanarayanan, D. Velayutham, J. Power Sources. **274**, 1135–1139 (2015)
13. J. Chu, G. Li, Y. Wang, X. Zhang, Z. Yang, Y. Han, T. Cai, Z. Song, A.C.S. Appl, Mater. Interfaces **14**, 25566–25575 (2022)
14. K. Zhang, C. Guo, Q. Zhao, Z. Niu, J. Chen, Adv. Sci **2**, 150018 (2015)
15. S. Dongmo, J. Witt, G. Wittstock, Electrochim. Acta **155**, 474–482 (2015)
16. J. Davis, M.T. Molina, C.P. Leach, M.F. Cardosi, A.C.S. Appl, Mater. Interfaces. **5**, 9367–9371 (2013)
17. Y.-F.C. Chau, C.-K. Wang, L. Shen, C.M. Lim, H.-P. Chiang, C.-T.C. Chao, H.J. Huang, C.-T. Lin, N.T.R.N. Kumara, N.Y. Voo, Sci. Rep **7**, 16817 (2017)
18. M.C. Pham, A. Hachemi, J.E. Dubois, J. Electroanal. Chem. **199**, 153–164 (1986)
19. J.-E. Dubois, P.-C. Lacaze, M.C. Pham, J. Electroanal. Chem. Interfacial Electrochem. **117**, 233–241 (1981)

20. M. Ferreira, H. Varela, R.M. Torresi, G. Tremiliosi-Filho, Electrochim. Acta. **52**, 434 (2006)
21. J. Ha, H. Soo, L. Hamenu, M. Latifatu, Y. Min, K. Man, J. Oh, W. Il, J. Myoun, J. Ind. Eng. Chem. **37**, 325 (2016)
22. M.M. Ardakani, P.E. Karami, H.R. Zare, M. Hamzehloo, Microchim. Acta. **159**, 165 (2007)
23. X. Liu, Z. Ding, Y. He, Z. Xue, X. Zhao, X. Lu, Colloids Surfaces B Biointerfaces. **79**, 27 (2010)
24. N. Akai, A. Kawai, K. Shibuya, J. Photochem. Photobiol. A Chem. **223**, 182 (2011)
25. M. Quan, D. Sanchez, M.F. Wasylkiw, D.K. Smith, J. Am. Chem. Soc. **129**, 12847 (2007)
26. T. Souier, S. Santos, A. Al Ghaferi, M. Stefancich, M. Chiesa, Nanoscale Res. Lett. **7**, 1 (2012)
27. Y. Gao, Nanoscale Res. Lett. **12**, 387 (2017)
28. P.L. Kronick, H. Scott, M.M. Labes, J. Chem. Phys. **40**, 890 (1964)

Authors and Affiliations

Kyuchul Lee[1] · Jihyun Hwang[2] · Jeong Ho Park[2] · Jongwook Park[3] · Kangwon Lee[1,4] · Jang Myoun Ko[2]

Jeong Ho Park
jongpark@khu.ac.kr

[1] Program in Nano and Technology, Graduate School of Convergence Science and Technology, Seoul National University, Seoul 08826, Republic of Korea

[2] Department of Applied Chemistry & Biotechnology, Hanbat National University, San 16-1, Dukmyung-Dong, Yusung-Gu, Daejeon 305-719, Republic of Korea

[3] Integrated Engineering, Department of Chemical Engineering, Kyung Hee University, Gyeonggi 17104, Korea

[4] Department of Applied Bioengineering, Graduate School of Convergence Science and Technology, Seoul National University, Seoul 08826, Republic of Korea